JOURNAL OF MATERIALS SCIENCE 27 (1992) 4341–4349

Imaging aerogels at the molecular level

G. C. RUBEN
Department of Biological Sciences, Dartmouth College, Hanover, NH 03755, USA
R. W. PEKALA, T. M. TILLOTSON, L. W. HRUBESH
Chemistry and Materials Science Department, Lawrence Livermore National Laboratory, Livermore, CA 94550, USA

Aerogels are a special class of open-cell foams that have an ultrafine cell/pore size (< 50 nm), high surface area (400–1000 $m^2 g^{-1}$), and an ultrastructure composed of interconnected colloidal-like particles or polymeric chains with characteristic dimensions of 10 nm. The purpose of this paper is to directly image a series of resorcinol–formaldehyde (RF) and silica aerogels by high resolution transmission electron microscopy (HRTEM). A new vertical replication technique allows us to examine aerogels at the molecular level *in situ* so that differences in polymeric and colloidal aerogels can be visualized. Such information is crucial for nano-engineering the structure and properties of these novel materials.

1. Introduction

The sol-gel polymerization of metal alkoxides or certain multifunctional organic monomers leads to the formation of highly cross-linked, transparent gels. If the solvent is simply evaporated from the pores of these gels, large capillary forces are exerted, and a collapsed structure known as a *xerogel* is formed. In order to preserve the gel skeleton, it is necessary to remove the aforementioned solvent under supercritical conditions. The low density, microporous material that results from this operation is known as an *aerogel.*

Aerogels have an ultrafine cell/pore size (< 50 nm), connected porosity, high surface areas (400–1000 $m^2 g^{-1}$), and an ultrastructure composed of interconnected colloidal-like particles or polymeric chains with characteristic dimensions of 10 nm. This ultrastructure is responsible for the unique optical, thermal, and acoustic properties of aerogels. For example, the ultrafine cell/pore size minimizes light scattering; and thus, aerogels are transparent porous solids. The high porosity of aerogels makes them excellent insulators with their thermal conductivity being approximately one hundred times lower than that of the fully dense matrix. Finally, the aerogel skeleton is responsible for the low sound velocities observed in these materials (i.e. 100–300 m s^{-1}) [1–3].

The most common aerogels are formed from the sol-gel polymerization of tetramethoxy silane (TMOS) or tetraethoxy silane (TEOS). Major variables in the polymerization include pH, $[H_2O]/[Si]$ ratio, type of alkoxy silane, and 1-step versus 2-step reactions. Under acidic conditions, hydrolysis is rapid and the Si–OH containing monomers slowly condense by cluster–cluster growth into linear or lightly branched polymer chains. These chains entangle and cross-link to form a gel that can be processed into a polymeric aerogel. In an alkaline environment, the condensation reaction is favoured and consumes any Si–OH containing monomers that are generated. These conditions promote the formation of highly branched silica species by monomer–cluster growth. Eventually, the clusters covalently link together through their surface silanol groups, leading to a gel that can be processed into a colloidal aerogel [4–6].

Organic aerogels are formed from the aqueous, sol-gel polymerization of resorcinol (1,3 dihydroxy benzene) with formaldehyde [7–10]. This reaction is conducted under alkaline conditions, with sodium carbonate as a base catalyst, and follows a monomer–cluster growth pathway. Organic aerogels are generally composed of interconnected spherical particles (3–20 nm) derived from highly branched clusters generated in solution. The [resorcinol]/[catalyst] ratio (R/C) is the principal variable that controls the size of the interconnected particles, leading to either polymeric or colloidal aerogels.

Numerous techniques (e.g. nuclear magnetic resonance, Brunauer–Emmett–Teller BET adsorption, SAXS, mechanical testing) have been used to characterize both silica and RF aerogels [11–15]. These data have led to the concept of polymeric and colloidal aerogels. In general, polymeric aerogels have high surface area, high stiffness, a fibrous ultrastructure, and a mass fractal dimension near 2.0. In contrast, colloidal aerogels have low surface area, low stiffness, an ultrastructure composed of interconnected spherical particles, and limited fractal characteristics. In reality, there is not a sharp dividing line between the characteristics of a polymeric and colloidal aerogel, rather a broad continuum is thought to exist.

While the above techniques indirectly probe the ultrastructure of an aerogel, the purpose of this paper is to directly image a series of RF aerogels and a base catalysed silica aerogel by high resolution transmission electron microscopy (HRTEM). A new vertical replication technique allows us to examine

0022–2461

aerogels at the molecular level so that differences in polymeric and colloidal aerogels can be visualized. Such information is crucial for tailoring the structure and properties of aerogels at the nanometer scale.

2. Experimental procedure

The preparation of RF gels has been described in detail [7]. Briefly, resorcinol and formaldehyde were mixed in deionized and distilled water at a molar ratio of 1:2 to give 5% w/v reactants. Sodium carbonate was then added as the base catalyst. After stirring, the RF solution was poured into glass vials that were tightly sealed and placed in a circulating oven for 7 days at 85–95 °C. The gels were then removed from their glass containers and placed in a dilute acid solution (0.12% trifluoroacetic acid). The acid treatment promoted additional cross-linking through the condensation of free hydroxymethyl ($-CH_2OH-$) groups.

In preparation for supercritical drying, the gels were exchanged into acetone. The solvent filled gels were placed in a jacketed pressure vessel (Polaron®) and covered with liquid CO_2. After sufficient exchanges with carbon dioxide to remove all acetone from the pores of the gel, the vessel was taken above the critical point ($T_C = 31$ °C; $P_C = 7.38$ Mpa). The samples were maintained at $\sim$ 50 °C for a minimum of 4 h, and then the pressure was slowly released through an exit valve. At atmospheric pressure, the wine-coloured aerogels were removed.

The silica gel was prepared from a methanol solution containing 0.83 M TMOS, 3.33 M water, and 0.078 M NH_4OH. The gel cured in approximately 2 h at 25 °C and was placed in an autoclave for supercritical extraction. The autoclave was slowly ramped to 280 °C to exceed the critical point of methanol ($T_C = 240$ °C; $P_C = 8.0$ Mpa). After venting the system, a transparent aerogel was removed.

The RF aerogels were prepared for HRTEM by fracturing them with a razor while submerged in a liquid nitrogen bath. In a few cases, the RF aerogels fractured spontaneously in liquid nitrogen without mechanical application of the razor. The fractured specimens remained transparent after evaporation of the liquid nitrogen due to its low surface tension. The silica aerogel was fractured with tweezers at room temperature because it was invisible in liquid nitrogen.

Next, the aerogel specimens were loaded onto the stage of a Balzers 300 freezing microtome, evacuated to 1.4 10^{-6} Pa, and cooled to $-$ 185 °C. The aerogels were platinum–carbon (Pt–C) replicated at an almost vertical angle (80°) and backed with a rotary deposited carbon film at a 100° angle. The thickness of the replica films is listed below:

Aerogel	R/C	Pt–C thickness (nm)	C film thickness (nm)
SiO_2	–	0.93	12.1
RF	50	0.93	12.3
RF	200	1.00	12.1
RF	300	0.93	12.1

The silica replica was removed from the aerogel with dilute HF, while the RF replicas were removed with concentrated Chlorox bleach. The replicas were floated (washed) on distilled water and then transferred to 300 or 400 mesh copper grids.

Aerogel replicas were imaged with a JEM 100CX TEM with a 262.5 nm depth of field and 0.66 nm resolution. The replica of mica was imaged on a JEM 2000 with a depth of field of 50 nm and a resolution of 0.48 nm. All samples were examined in stereo with a tilt series at 10^4–10^5 magnification. Kodak 4489 film was used and image reversals and prints were made as previously described [16].

From previous work, a 0.93 nm thick Pt–C film increases the average polysiloxane chain of $\sim$ 0.41 nm by roughly 0.56 nm to a Pt–C coated average thickness of 0.97 nm [17, 18]. It is assumed that the average unbranched RF chain thickness is between 0.4–0.7 nm and its width is increased by a 0.93 or 1.00 nm thick Pt–C film by 0.56 or 0.6 nm. A Pt–C coated RF chain should average between 0.9–1.3 nm which is the chain size found in all the Pt–C replicated RF aerogels.

Colloidal beads or particles in the aerogel preparations were identified with stereoimages and then measured. The direction perpendicular to the connector axis was measured because bead edges within the connector were in general not visible.

3. Results and discussion

The structure and properties of RF aerogels are largely determined by the amount of catalyst used in the sol-gel polymerization. Because the pH of the reaction decreases as the polymerization proceeds, each formulation is referenced by the [resorcinol]/[catalyst] ratio in the mixture. R/C ratios of 50–300 provide an acceptable range for the production of transparent gels and aerogels.

Resorcinol reacts with formaldehyde under alkaline conditions to form a mixture of addition and condensation products. These intermediates further react to form a cross-linked polymer network. The two major reactions include: (a) the formation of hydroxymethyl ($-CH_2OH$) derivatives of resorcinol, and (b) the condensation of the hydroxymethyl derivatives to form methylene ($-CH_2-$) and methylene ether ($-CH_2OCH_2-$) bridged compounds [19–21]. One major difference between the RF and silica sol-gel polymerizations is that resorcinol is only a trifunctional monomer whereas TMOS is tetrafunctional. Fig. 1 shows a schematic diagram of both polymerizations.

Table I summarizes the density, pore size, and surface area for the aerogels examined in this study. Although the RF gels were prepared at the same concentrations (5% w/v reactants), the final aerogel densities depend upon the R/C ratio. Under high catalyst conditions (i.e. R/C = 50), a large amount of shrinkage is experienced during supercritical drying, leading to a higher density aerogel. The relationship between the final aerogel density and the R/C ratio is not linear. At R/C $\geqslant$ 150, the final densities plateau at a value $\sim$ 15% higher than the target value. Some

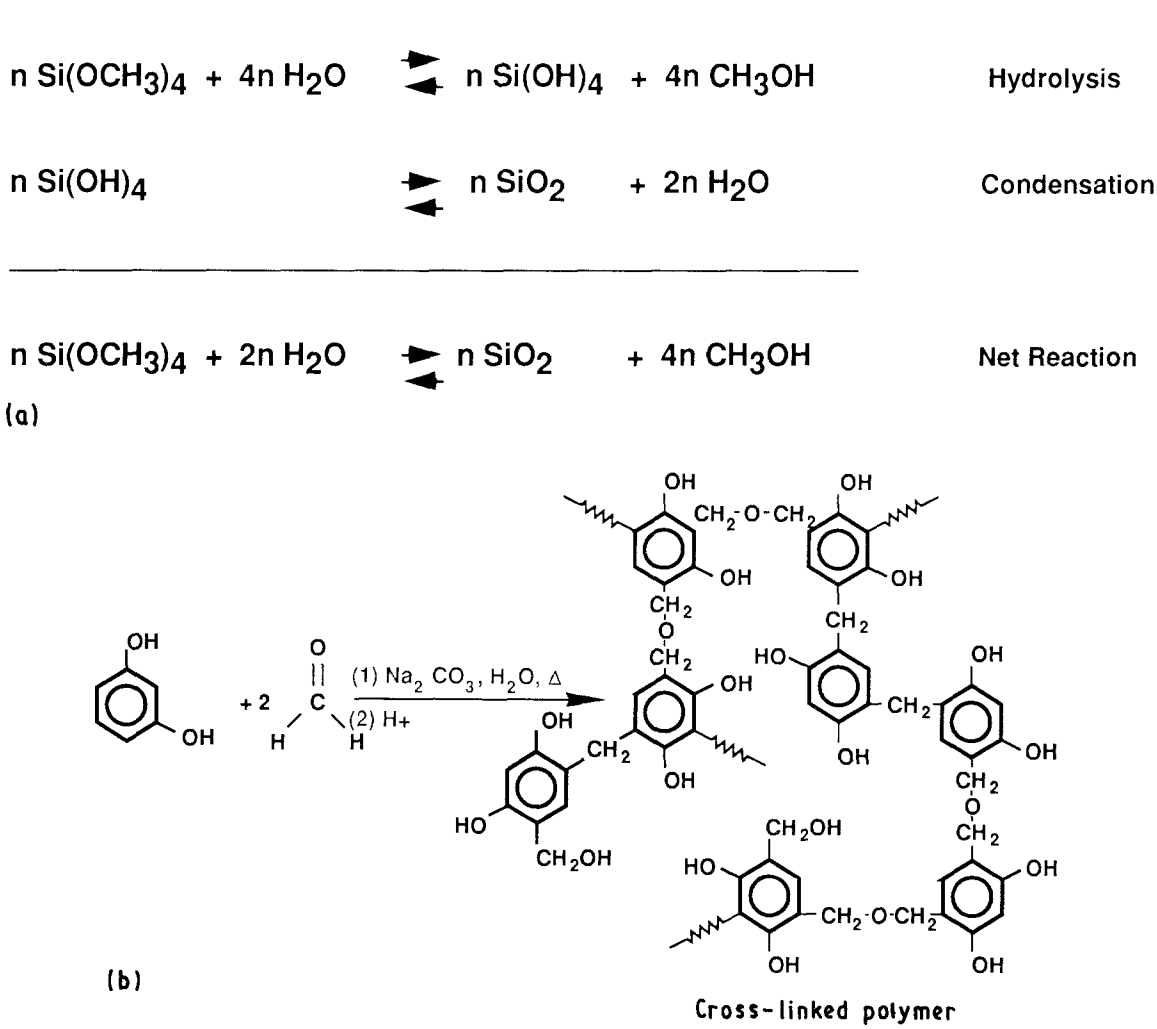

Figure 1 Schematic diagram of the sol-gel polymerization of: (a) tetramethoxy silane [TMOS] and (b) resorcinol with formaldehyde into covalently linked aerogels.

TABLE I Aerogel data

ID	R/C	Catalyst	Density (g cc^{-1})	SA_{BET} (m^2 g^{-1})	Mean pore radius, R_G, (nm)
RF	50	Na_2CO_3	0.103	905	7.05
RF	200	Na_2CO_3	0.063	577	10.30
RF	300	Na_2CO_3	0.065	389	13.47
SiO_2	–	NH_4OH	0.065	594	–

Note: R_G was determined from small angle X-ray scettering.

shrinkage also occurs in the case of the silica aerogel and its density is ~ 20% higher than the target value.

The BET surface area and compressive modulus of RF aerogels show an inverse relationship with the R/C ratio. The aerogel prepared under high catalyst conditions (i.e. R/C = 50) has a higher surface area and compressive modulus than its low catalyst counterparts (i.e. R/C = 200 or 300). The surface area of the silica aerogel is comparable to the RF aerogel synthesized at R/C = 200.

Fig. 2 shows the compressive modulus of the RF and silica aerogels as a function of density and catalyst conditions [22–24]. As expected, the modulus increases as a function of aerogel density. The linear log–log plot in each case demonstrates a power-law density dependence that has been observed in many other low density foams. This relationship is expressed as

$$E = c\rho^n \quad (1)$$

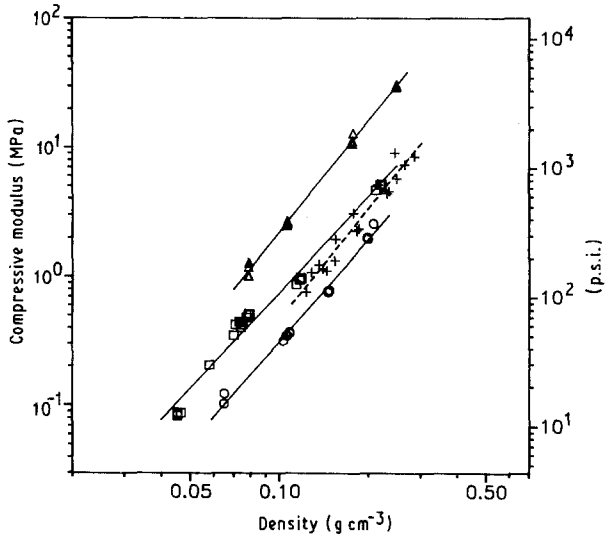

Figure 2 A log-log plot of compressive modulus versus density for: (———) resorcinol–formaldehyde aerogels (R/C = (△) 50; (□) 200; (○) 300) and (– – –) silica aerogels: (+) base catalysed.

where ρ is the bulk density, c is a constant (prefactor), and n is a non-integer exponent that ranges from 2–4. For most open-cell and closed-cell foams, this exponent usually falls very close to 2.0 and 3.0, respectively. Foams with irregular, fractal morphologies generally have a value that exceeds 3.0 [15, 25, 26].

In the case of RF aerogels, the above exponent equals 2.7 ± 0.2 for all formulations. Although the scaling exponents are the same, the prefactors scale inversely with the R/C ratio. This relationship is associated with differences in the inter-particle connectivity of the RF aerogels. At equivalent densities, RF aerogels prepared at R/C = 50 are approximately seven times stiffer than RF aerogels prepared at R/C = 300. Base catalysed silica aerogels have a nearly identical scaling exponent (2.9 ± 0.2) to the RF aerogels. In addition, their moduli fall between that of the RF aerogels prepared at R/C = 200 and 300.

The effects of the R/C ratio upon the density, surface area, and mechanical properties of organic aerogels suggest differences in their ultrastructure. Nevertheless, some similarities with the base catalysed silcia aerogel can also be observed. Based upon the above information, only the RF aerogel synthesized at R/C = 50 would be considered polymeric with all other aerogels regarded as colloidal. Previous TEM studies have shown differences in the interconnected particle size of the RF aerogels. These studies, however, suffered from an inability to examine the *in situ* aerogel structure at the molecular level because a thin layer of isolated aerogel was spread on a support film for observation with the inherently low contrast and poor resolution of this technique.

Before examining the high resolution TEMs of this study, it is necessary to define terminology and demonstrate the resolution of the technique. Fig. 3 shows a schematic diagram of the ultrastructure of a hypothetical aerogel. In general, we discuss connectors that run between cross-linking junctions. The connectors can be composed of distinct colloidal-like particles or twisted ladder-like chains having irregular-spaced steps. A connector will rarely be longer than 100 nm in size before it meets with other connectors to form a cross-linking junction. As will be demonstrated, we are able to look inside the connectors and resolve individual RF or siloxane chains.

Fig. 4 shows images of a replicated mica surface, three different RF aerogels, and a silica aerogel at 1 490 000x. The filamentous granularity of the 80° replicated mica surface is 0.5 nm, setting a lower bound for our resolution, and permitting us to resolve a 1.0 nm step in the mica. The structure of the vertically replicated 0.97 nm Pt–C film on mica demonstrates that the granularity of the deposited film cannot account for the structures (polymer chains) observed in the RF or silica aerogels. Ruben has previously shown that this technique can resolve both single strands in the DNA double helix [16].

In Fig. 5a, the surface of the silica aerogel is shown at 528 000x. It is important to study this aerogel with a 10x magnifier so the silica chains can be observed within the connectors. In Fig. 5b it is possible to observe Fig. 5a in three dimensions using stereo glasses (2x magnification). The aerogel connectors in Fig. 5a and b contain many small spherical particles or beads (see arrows). The beads range in size from 8.6–13.2 nm with an average diameter of 11.3 ± 1.0 nm. The connectors often have a string of pearls morphology (see lower parallel arrows in Fig. 5b). Furthermore, it was not uncommon to find

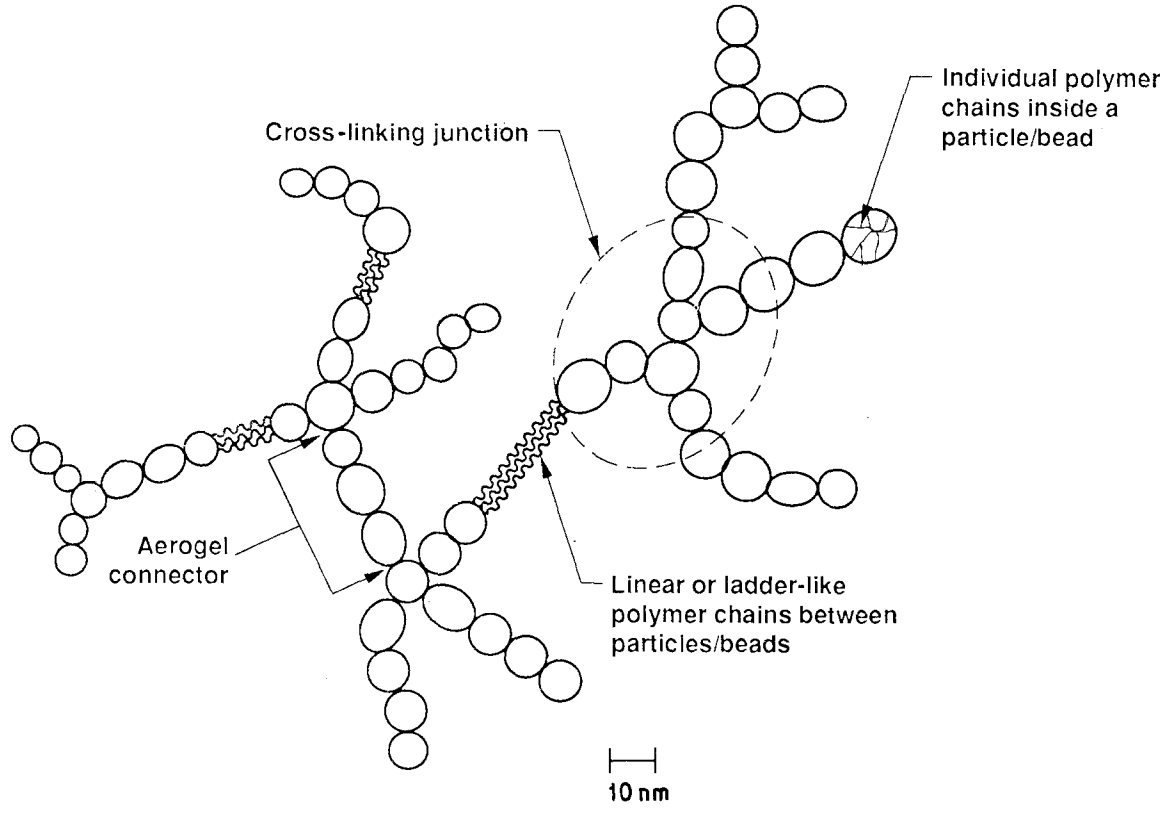

Figure 3 Schematic diagram of the ultrastructure of a hypothetical aerogel.

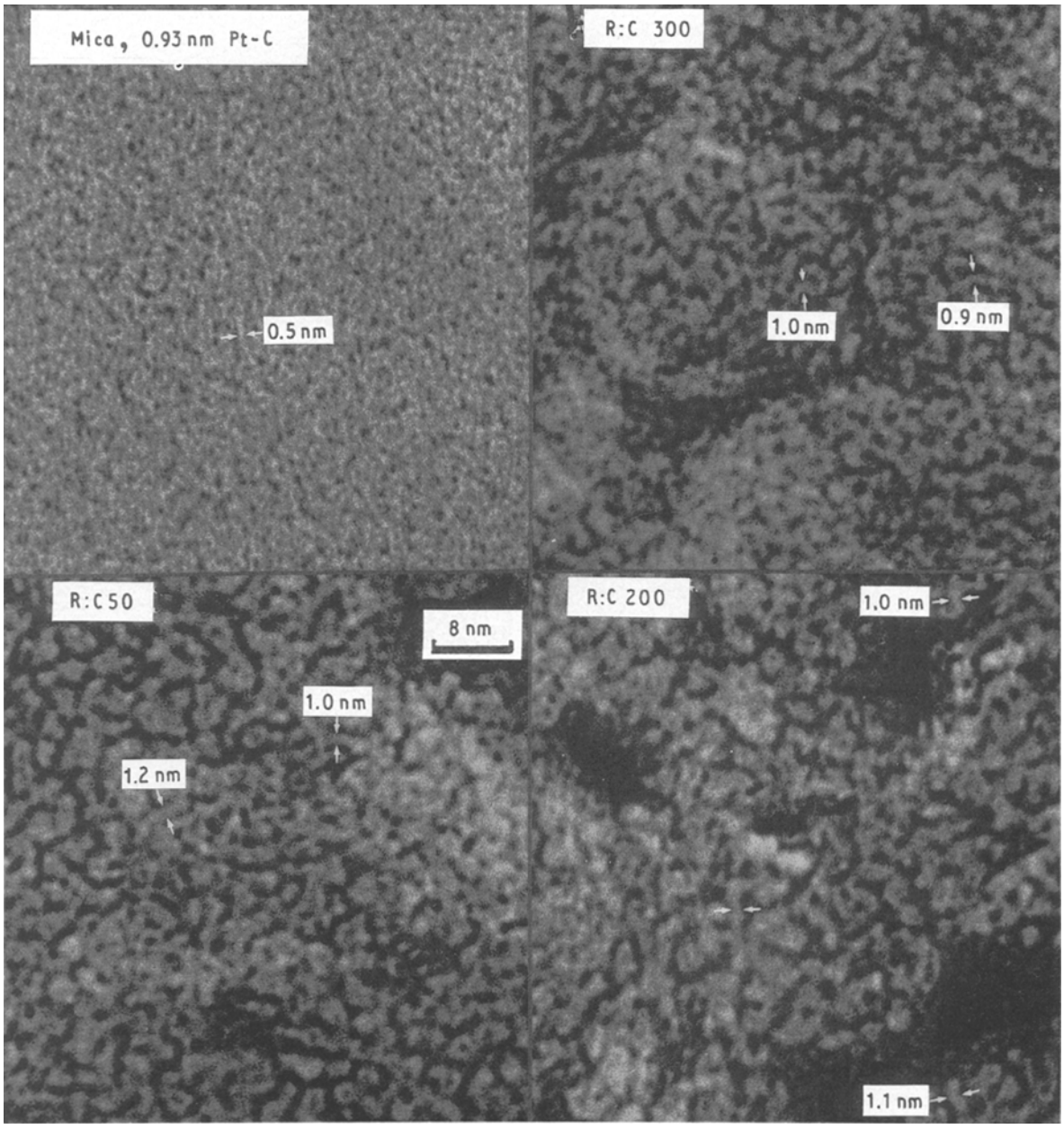

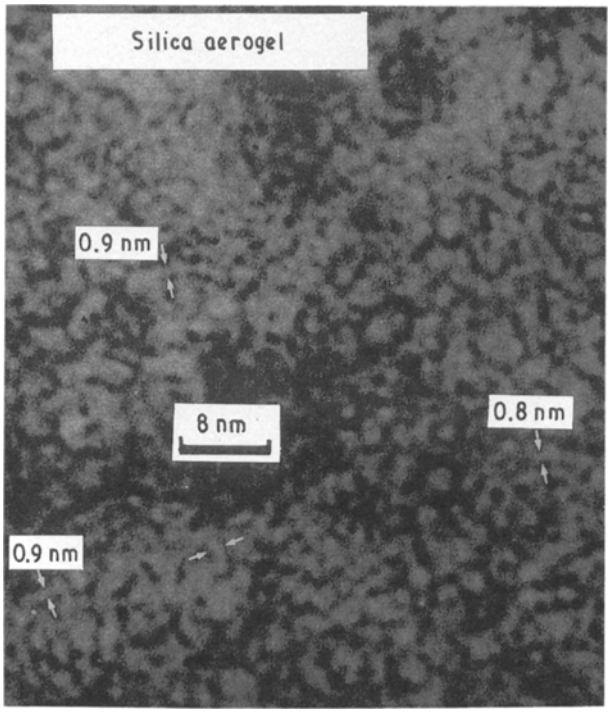

Figure 4 This composite image contains five separate panels: mica, three resorcinol–formaldehyde (RF) aerogels produced with [resorcinol]/[catalyst] ratios of 50, 200, and 300, and a silica aerogel. Each surface was cooled to − 185 °C and vertically (80°) replicated with 0.93–1.0 nm Pt–C and backed with 12.1–12.3 nm of rotary deposited carbon. The RF and silica aerogel surfaces contain 0.9–1.3 nm wide Pt–C coated resorcinol–formaldehyde polymer chains and 0.9 nm wide silica chains. The same Pt–C coating on mica produces Pt–C filamentous structures of ~ 0.5 nm width. This clearly demonstrates that the Pt–C coated resorcinol–formaldehyde chains (0.4–0.7 nm wide) and silica chains (~ 0.41 nm) increased by 0.5 nm to 0.9–1.3 nm are easily distinguished from the ~ 0.5 nm noise level of the 0.93 nm Pt–C film. Magnification 1 490 000x.

adjacent beads joined by 2–4 Pt–C coated siloxane chains and separated by 1–5 bead diameters. Such a connection is visible between beads shown at the upper left in Fig. 5b. The arrows in Fig. 5c show two siloxane chains looping around each other.

Based upon the preponderance of beads making up the silica ultrastructure, it is not surprising that this material would be considered a colloidal aerogel. It should be noted that this replica still contains some

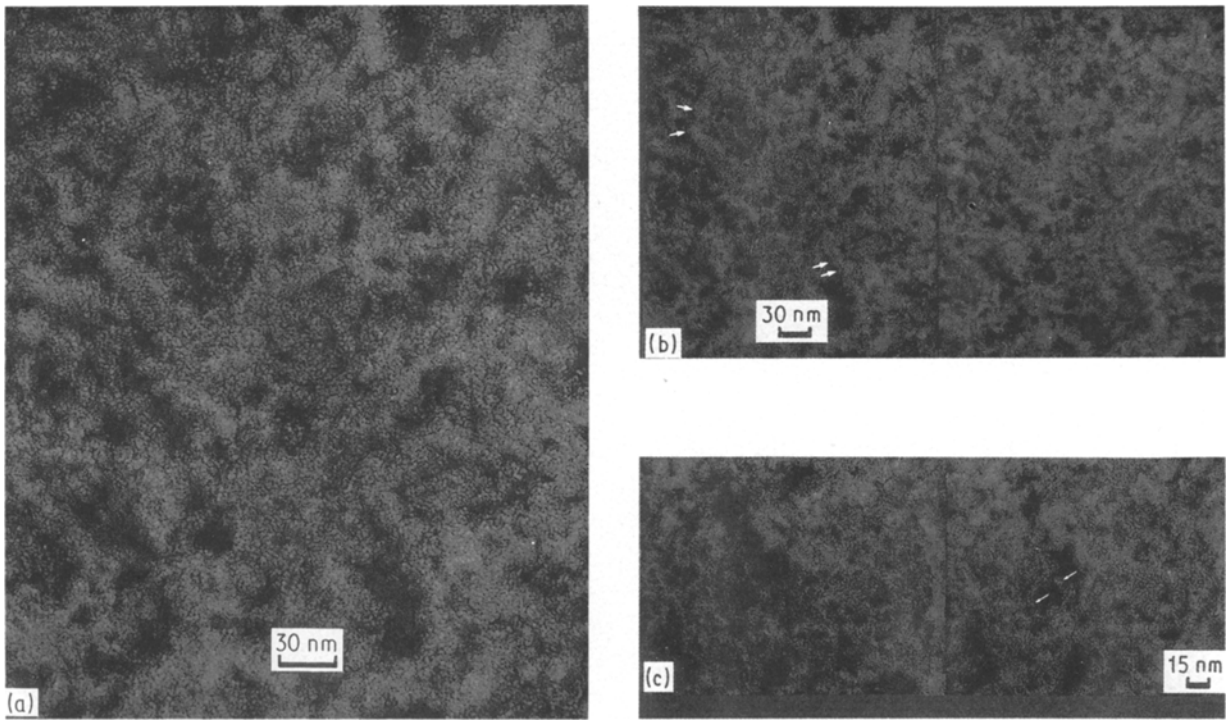

Figure 5 (a) This image of a base catalysed silica aerogel contains features of the aerogel schematically diagramed in Fig. 3. In order to understand the construction of this aerogel it should be viewed with an eye loop (10x) at the molecular level and observed in stereo in Fig. 5b, magnification 528 000x. (b) This pair of stereoscopic images (tilt angle of 10°) of a silica aerogel is composed of connectors with beads averaging 11.3 ± 1 nm (parallel arrows at lower left) which are occasionally separated by 10–60 nm and bonded by small numbers (3–7) of polymeric chains (between arrows at upper left), magnification 205 000x. (c) This stereopair (10° tilt angle separation) of the silica aerogel shows a number of polymeric connectors at the left of centre composed of 1–4 silica chains. At the right side of the image, the connectors are composed as in Fig. 5a of beads and polymeric chains, magnification 267 000x.

unremoved silica which is probably responsible for its low contrast. While low contrast does not affect image resolution, it makes the beads and siloxane chains harder to see.

Fig. 6a–d show HRTEM images of the RF 50 aerogel prepared at R/C = 50. In contrast to the silica aerogel, this aerogel contains very few spheroidal particles or beads. For the few beads that were observed, they ranged in size from 9.3–16.6 nm with an average diameter of 12.0 ± 3.0 nm. At first glance, the connectors in this material (3.0–13.5 nm) in Fig. 6b appear to have widths similar to the silica aerogel connectors (2.5–13.2 nm). The 203 000x magnification stereopair in Fig. 6b does not fully resolve the connector substructure but it gives a good 3-D topographical view of the aerogel area in Fig. 6a.

To fully resolve the connector substructure, it was necessary to examine RF 50 in stereo at 333 000x magnification with tilt angles of 10° and 15° between stereopairs (Fig. 6c and d). In general, the connectors were composed of branched and highly convoluted resorcinol–formaldehyde chains that formed filaments with diameters of 2–6 nm. The open morphology of the connectors explains the high surface area of this aerogel. In our current model of the RF polymerization, we believe that at R/C = 50, numerous small clusters (~ 3 nm) are linked together in solution to form the gel structure. HRTEM suggests that such small particles may exist during the early stages of polymerization; however, extensive molecular chain growth or interpenetration makes the beads indistinguishable in the dried aerogel. The images in Fig. 6c and d as well as the indirect physical measurements and high surface area characterize RF 50 as a polymeric aerogel.

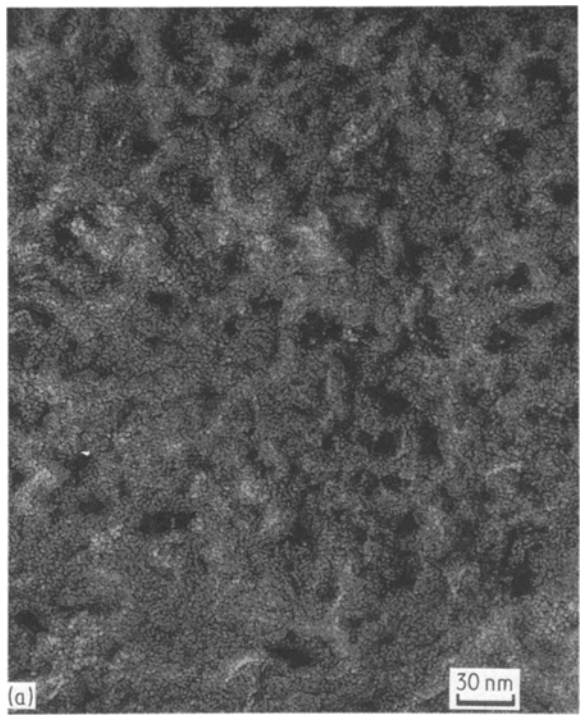

Figure 6 (Continued)

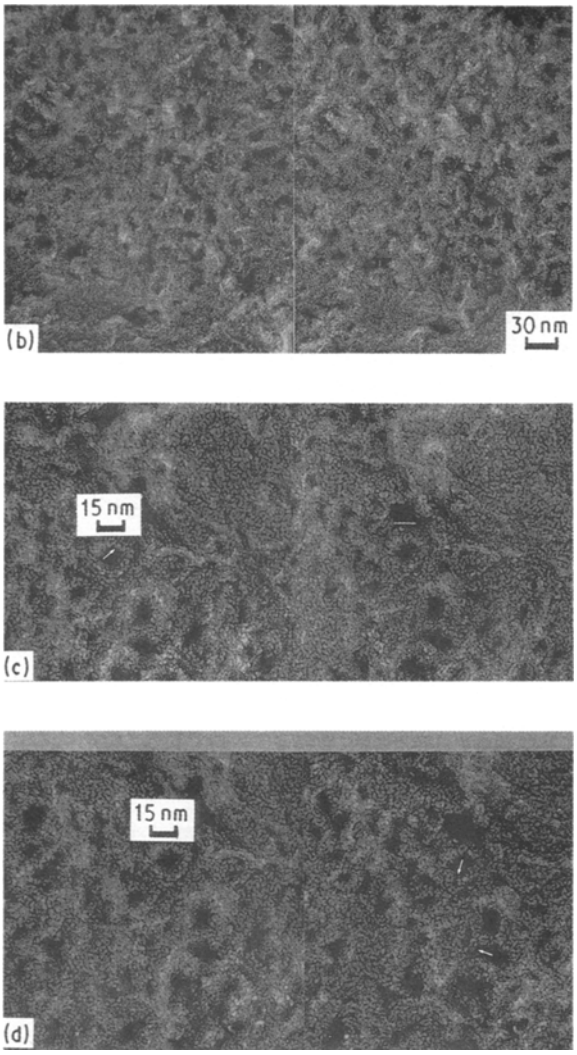

Figure 6 (a) This image of the RF 50 aerogel (R/C = 50) demonstrates a very high density of connectors. Although its bulk density is ~ 60% greater than the other RF aerogels, this aerogel has thinner connectors (3.0–13.5 nm) and therefore has a greater frequency of connectors on a mass basis than RF 200 or RF 300. The connectors are composed of branched resorcinol–formaldehyde chains that form filaments with diameters of 2–6 nm, magnification 543 000x. (b) These stereoimages (tilt angle of 10°) of the same RF 50 aerogel area in Fig. 6a are composed of large and small non-colloidal connectors extending between junctions. This stereoimage confirms the general lack of spheroidal bead subunits in Fig. 6a, magnification 203 000x. (c) This stereopair (tilt angle of 10°) of RF 50 shows the same area that follows in Fig. 6d from a slightly different perspective and with less apparent depth due to a smaller tilt angle. Fig. 6d and this stereoimage suggest that the high catalyst concentration creates small, branched polymer clusters that condense to form filaments *via* extensive molecular chain interpenetration (see arrow), magnification 333 000x. (d) This stereopair (tilt angle of 15°) of RF 50 shows connectors made up of thin RF filaments as described in Fig. 6c. None of the other aerogels contain connectors composed of such highly branched, thin filaments (see arrows), magnification 333 000x.

The RF aerogel synthesized at R/C = 200 is shown in Fig. 7a–d. This colloidal aerogel contains easily recognizable spheroidal beads with diameters ranging from 13–15 nm and averaging 14 ± 1 nm. RF 200 connectors frequently appear to have a string of pearls morphology with slightly larger beads than the silica aerogel. The spheroidal beads in the RF 200 connectors, in contrast to the silica aerogel, are more strongly joined with interbead RF chains covering a cross-sectional area generally larger than the bead's radius.

In Fig. 7a–d there are also a few connectors composed of 2–6 interlaced, polymer chains. These chains can sometimes extend 40–60 nm between junctions. In Fig. 7b and c cross-linking junctions composed of three, four, and five aerogel connectors can be seen. A junction with five connectors is highlighted by an arrow in Fig. 7c. The spheroidal beads and connector substructure are clearly visible in Fig. 7d. The beads are microporous (0.6–2.5 nm) and the chains in their surface are larger than single RF chains. These images suggest that there are many branched chains closely associated in the surface. In numerous ways, this organic aerogel is the structural analogue of the base catalysed silica aerogel.

At R/C = 300, the resultant RF aerogel is more obviously colloidal than any of the other aerogels (Fig. 8a). The interconnected spheroidal beads are quite polydisperse with sizes ranging from 16–30 nm and with an average diameter of 21 ± 3 nm. Because of the larger bead size, almost all the connectors look like a string of pearls with some connectors as long as 10–12 beads. The beads appear to be attached over a

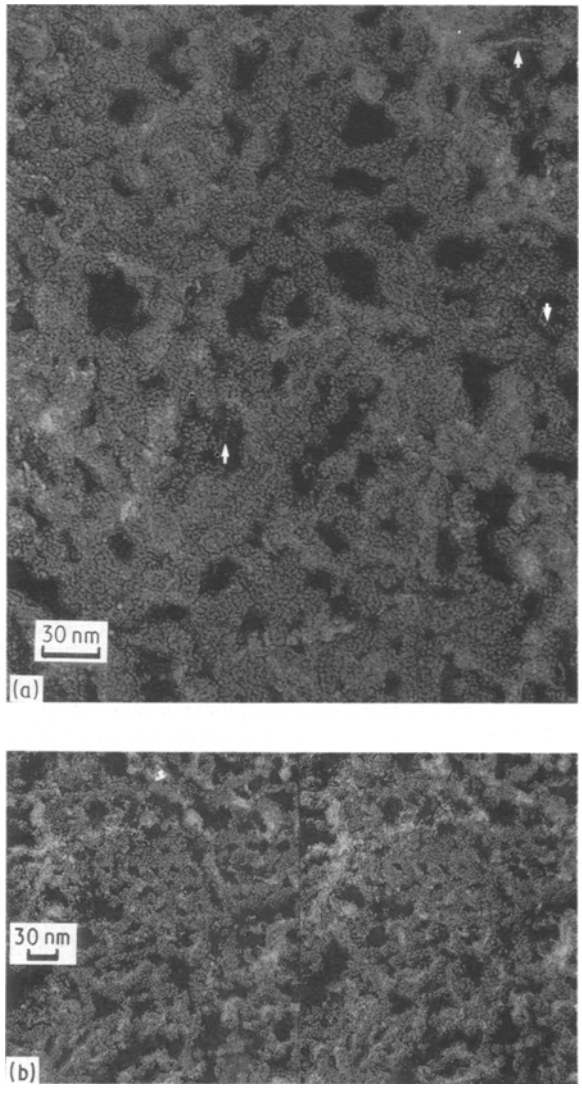

Figure 7 (Continued)

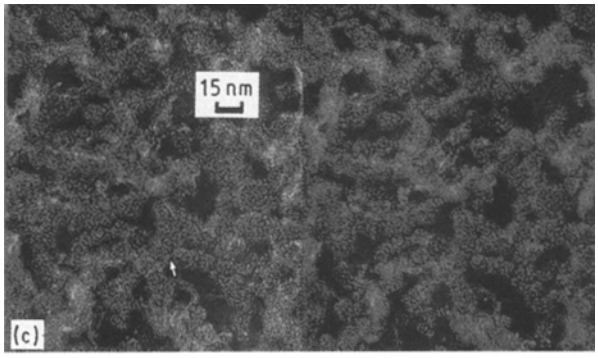

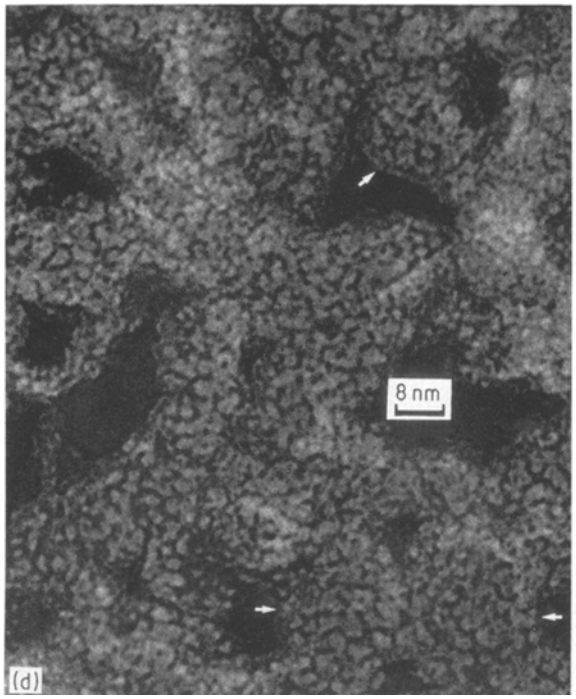

Figure 7 (a) This RF 200 aerogel network (R/C = 200) is formed from connectors and junctions of condensed beads (~ 14 ± 1 nm), where the beads are usually interconnected by resorcinol–formaldehyde chains over an area defined by at least half the diameter of the bead. In addition there are thinner polymeric connectors marked with arrows, magnification 542 000x. (b) This stereopair (tilt angle of 5°) of the RF 200 aerogel demonstrates that three, four, and five connectors frequently join together to form junctions. RF 200 has the characteristics of a colloidal aerogel with bead surfaces that are molecularly rough (~ 1–3 nm range) and microporous (0.6–2.5 nm), magnification 208 000x. (c) This stereopair (tilt angle of 5°) of RF 200 shows connectors made up of colloidal beads (~ 14 ± 1 nm). This image shows the relatively rare intersection of ~ 5 connectors to form a junction (see arrow), magnification 333 000x. (d) This image of the RF 200 aerogel not only shows microporous colloidal beads (see arrows) composed of branched resorcinol–formaldehyde chains terminating at the bead surface, but it also shows a connector (~ 6 nm across) at the left of centre composed of a small group of polymeric chains. This polymeric connector is also shown at the bottom right of the stereoimages in Fig. 7c, magnification 1 725 000x.

cross-sectional area generally defined by less than a bead's radius (Fig. 8b). This loosely bonded ultrastructure explains the weak mechanical behaviour of the aerogel. By observing the surface of the spheroidal beads with the stereoimages in Fig. 8c, the chains on the surface of the beads appear to be single (0.9–1.3 nm) and are not closely associated as they are in RF 200. The spheroidal beads in Fig. 8c and d are microporous (0.5–3.0 nm) with pore sizes similar to those in RF 200.

These first ever stereoscopic images have made it possible to interpret the relationship between structure and properties in aerogels at the molecular level. This new vertical replication technique for TEM is an extraordinary tool for understanding sol-gel chemistry and the resultant materials. Our results clearly show that the terms polymeric and colloidal, as applied to aerogels, do not simply represent two structural extremes. Instead, a complex mixture of ultrastructural units (e.g. spheroidal beads, helices) is found in each type of aerogel.

4. Summary

HRTEM has been used to examine a series of RF aerogels and a base catalysed silica aerogel. This technique has provided us with molecular information about the aerogels, and it has enabled us to distinguish a polymeric aerogel from its colloidal counterparts.

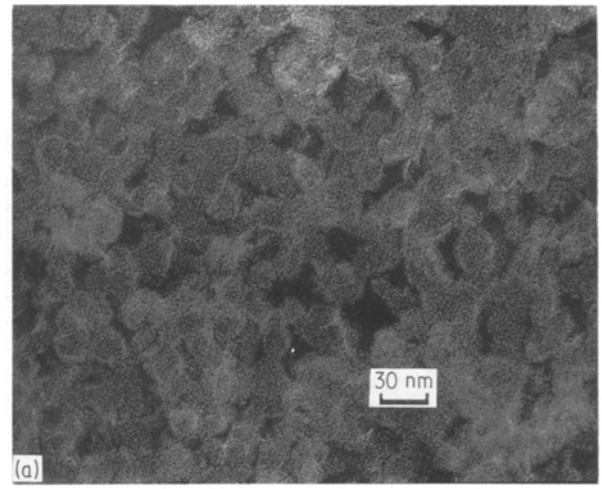

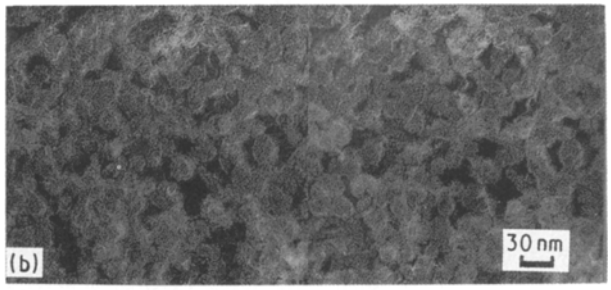

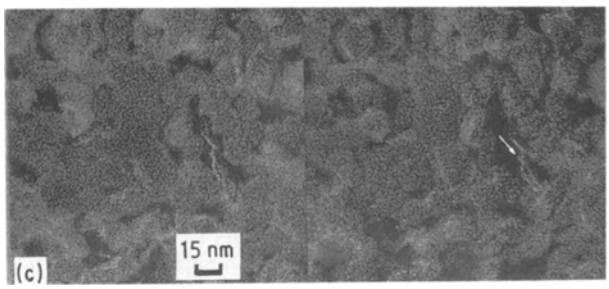

Figure 8 (Continued)

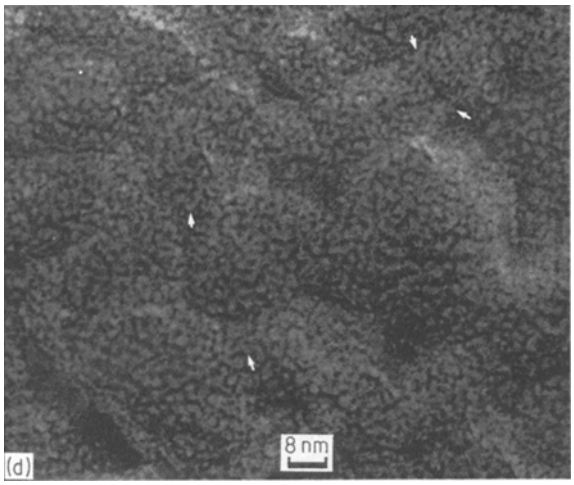

Figure 8 (a) This RF 300 aerogel network (R/C = 300) is formed from connectors and junctions of condensed beads (~ 21 ± 3 nm) where the beads are usually interconnected by resorcinol–formaldehyde chains over an area defined by less than half the diameter of the bead, magnification 528 000x. (b) This stereopair (tilt angle of 5°) of the RF 300 aerogel demonstrates that three and four connectors frequently meet at junctions, magnification 200 000x. (c) This stereopair (tilt angle of 10°) of the RF 300 aerogel shows connectors made up of colloidal beads (~ 21 ± 3 nm). This RF 300 aerogel is colloidal with bead surfaces that appear molecularly rough (~ 1–3 nm range) and microporous (0.5–3 nm). The resorcinol–formaldehyde chains do not appear as thick as the chains on the surface of the RF 200 and RF 50 aerogels. The thicker chains are thought to be due to more frequent chain branching. The thin connector to the right of centre (see arrow) has a diameter of 2 nm and is polymeric in character, magnification 337 000x. (d) This image of the RF 300 aerogel shows a grouping of microporous colloidal beads composed of mostly unbranched resorcinol–formaldehyde chains terminating at the surface of the beads. There are also small numbers of polymeric resorcinol–formaldehyde chains (see arrows) extending between particles, magnification 1 670 000x.

The ability to tailor the structure and properties of aerogels at the nanometer level presents some exciting opportunities for these microporous materials. We believe that HRTEM can serve as an important tool in the development of improved sol-gel polymerizations by linking the chemistry, structure, and properties of aerogels at the molecular level.

Acknowledgements

This work was partially performed under the auspices of the US Department of Energy by Lawrence Livermore National Laboratory under Contract #W-7405-ENG-48. We thank Blanca Haendler for arranging this collaboration and Dartmouth's Rippel Electron Microscope facility for use of its equipment.

References

1. "Aerogels", edited by J. Fricke (Springer-Verlag, New York, 1986).
2. J. FRICKE, *Sci. Amer.* **258** (1988) 92.
3. *Idem*, in "Sol-Gel Science and Technology", edited by M. A. Aegerter, M. Jafelicci, D. F. Souza and E. D. Sanotto (World Science Publishers, New Jersey, 1989) p. 482.
4. C. J. BRINKER and G. W. SCHERER, in "Sol-Gel Science" (Academic Press, New York, 1990).
5. *Idem, J. Non-Cryst. Solids* **70** (1985) 301.
6. See "Better Ceramics Through Chemistry I–IV", *Mater. Res. Soc. Proc.* **32, 73, 121, 180** (1984, 1986, 1988, 1990).
7. R. W. PEKALA, *J. Mater. Sci.* **24** (1989) 3221.
8. R. W. PEKALA and F. M. KONG, *J. de Physique Coll. Suppl.* **50** (1989) C4–33.
9. *Idem, Polym. Prpts.* **30** (1989) 221.
10. R. W. PEKALA, *Mater. Res. Soc. Proc.* **171** (1990) 285.
11. D. W. SCHAEFER, J. P. WILCOXON, K. D. KEEFER, B. C. BUNKER, R. K. PEARSON, I. M. THOMAS and D. E. MILLER, in "Physics and Chemistry of Porous Media II", edited by J. R. Banavar, J. Koplik, K. W. Winkler, AIP Conference Proceedings **154** (1986) 1.
12. D. W. SCHAEFER, *Science* **243** (1989) 1023.
13. A. CRAIEVICH, M. A. AEGERTER, D. I. DOS SANTOS, T. WOIGNIER and J. ZARZYCKI, *J. Non-Cryst. Solids* **86** (1986) 394.
14. L. W. KELTS and N. J. ARMSTRONG, *J. Mater. Res.* **4** (1989) 423.
15. T. WOIGNIER, J. PHALIPPOU and R. VACHER, *ibid.* **4** (1989) 688.
16. G. C. RUBEN, *J. Elect. Microsc. Tech.* **13** (1989) 335.
17. M. W. SHAFER, D. D. AWSCHALOM, J. WARNOCK and G. C. RUBEN, *J. Appl. Phys.* **61** (1987) 5438.
18. G. C. RUBEN and M. W. SHAFER, *Mater. Res. Soc. Proc.* **73** (1986) 207.
19. D. D. WERSTLER, *Polymer* **27** (1986) 757.
20. A. SEBENIK, U. OSREDKAR and I. VIZOVISEK, *ibid.* **22** (1981) 804.
21. R. W. PEKALA and R. L. WARD, *Polym. Prpts.* **31** (1990) 167.
22. J. D. LEMAY, R. W. PEKALA and L. W. HRUBESH, *Pacific Polym. Prpts.* **1** (1989) 295.
23. R. W. PEKALA, C. T. ALVISO and J. D. LEMAY, *J. Non-Cryst. Solids* **125** (1990) 67.
24. J. D. LEMAY, T. M. TILLOTSON, L. W. HRUBESH and R. W. PEKALA, *Mater. Res. Soc. Proc.* **180** (1990) 321.
25. L. J. GIBSON and M. F. ASHBY, *Proc Royal Soc. Lond.* **382(A)** (1982) 43.
26. E. A. MEINECKE and R. C. CLARK, in "Mechanical Properties of Polymeric Foams" (Technomic Publications, CT, 1973).

Received 9 April
and accepted 1 August 1991